Available online www.jocpr.com

Journal of Chemical and Pharmaceutical Research, 2016, 8(3):281-288

Research Article

ISSN : 0975-7384
CODEN(USA) : JCPRC5

Investigation on influence of fluorine substitution on structural, thermal and *in-vitro* behaviour of nanodimensional hydroxyapatite

Seema Kapoor[a]*, Uma Batra[b] and Kohli Suchita[a]

[a]*Dr. SSB University Institute of Chemical Engineering & Technology, Panjab University, Chandigarh, India*
[b]*Department of Materials & Metallurgical Engineering, PEC University of Technology, Chandigarh, India*

ABSTRACT

In this study, hydroxyapatite (HA, $Ca_{10}(PO_4)_6(OH)_2$) and fluorine-substituted hydroxyapatite (FHA, $Ca_{10}(PO_4)_6OHF$) nanopowders were synthesized through water based sol-gel technique using a novel phosphorous precursor. Transmission Electron Microscopy (TEM), BET Surface Area, X-ray Diffraction (XRD), Fourier Transform Infrared Spectroscopy (FTIR) and Thermogravimetry (TGA)/Differential Thermogravimetry (DTG) techniques were employed in order to evaluate characteristics of nanopowders. The in-vitro study of nanopowders was assessed in simulated body fluid (SBF) maintained at 37°C. The band assigned to OH---F---OH present in FTIR spectrum of FHA at 721 cm^{-1} confirmed the substitution of fluorine in HA lattice. The fluorine substitution was found to alter the morphology and structural parameters of apatite crystals. It also significantly lowered the BET surface area. FHA nanopowder had improved thermal stability as compared to HA in the temperature range 25°C to 1600°C. The bioactivity assay confirmed formation of an amorphous calcium phosphate layer on the surface of nanopowders after immersion in SBF solution.

Keywords: Hydroxyapatite; fluorine substitution; nanopowders; BET surface area; *in-vitro*.

INTRODUCTION

Hydroxyapatite (HA) is a major mineral component of the calcified tissues (i.e. bones and teeth) and is being extensively used as the most hopeful hard tissues substitute material due to its similarity to natural bone in crystalline structure, chemical composition, bioactivity, and biocompatibility [1]. Synthetic HA has been used for a variety of other biomedical applications like matrices for controlled drug release, bone cements, tooth paste additive, dental implants etc. [2-4]. The bioactive HA phase has been most widely researched due to its outstanding biological response to the physiological environment. However, there is a significant difference of properties between natural apatite crystal found in the bone mineral and the conventional synthetic HA. The bone mineral also contains trace ions such as cations (Zn^{2+}, Na^{+}, Mg^{2+}, K^{+}, Mn^{2+}, Sr^{2+}) or anions (F^{-}, Cl^{-}, HPO_4^{2-}, SiO_4^{4-} or CO_3^{2-}) [5]. The incorporation of physiologically relevant ions into the hydroxyapatite structure can affect its physical and chemical properties such as crystallinity, thermal stability, solubility and osteoconductivity [6] and improve its biocompatibility and bioactivity [7]. Among these ions, the presence of fluorine (F^{-}) in saliva and blood plasma is important for normal skeletal and dental development. Its substitution in HA improves the bond between the bone and the implant [8] and strengthens the bone structure [9]. As it provides the low solubility, demineralization of bone is prevented. The thermal stability of HA is enhanced by its substitution and it also induces a better biological response [10]. When OH^{-} lattice positions in HA are partially substituted by F^{-}, fluorine substituted hydroxyapatite (FHA, $Ca_{10}(PO_4)_6OH_{2-x}F_x$, $0 < x < 2$) is obtained. If substitution is completed, fluorapatite (FA, $Ca_{10}(PO_4)_6F_2$) is formed, which is not osteo-conductive [11]. For the best dissolution and resistance and cell activities, it is recommended that the molar level of fluorine ion should be in the range 0.8 to 1.1 [12].

Many methods have been developed, namely, precipitation, [10, 11, 13], ethanol based sol-gel, [14-16], solid state

reaction [17], hydrothermal, [18,19], pH cycling [20-22], mechanical alloying method [23] and microwave processing [24] for the synthesis of nanopowders at different pH conditions, using diammonium hydrogen phosphate or phosphorous pentaoxide as phosphorous precursor. But no research has reported the use of potassium dihydrogen phosphate as phosphorous precursor, which is freely soluble in water and is not toxic compared to the above mentioned phosphorous precursors. The effect of fluorine substitution on surface area and *in-vitro* behaviour has seldom been studied systematically. Bianco et al. [13] and Nathanael et al. [18] have reported surface area of FHA nanopowders synthesized by precipitation and hydrothermal method, respectively.

As per available literature, the synthesis of FHA nanopowder by water based sol-gel method and systematic investigation on influence of fluorine on structural, thermal and *in-vitro* behaviour of nanodimensional hydroxyapatite has not been reported. Thus the aim of this study was to examine in detail the structural features (crystallite size, crystallinity, morphology, surface area), thermal and *in-vitro* behaviour of HA and FHA nanopowders synthesized using water based sol-gel technique.

EXPERIMENTAL SECTION

2.1. Synthesis of HA and FHA

Nanodimensional HA and FHA powders were synthesized by sol-gel route. Nominal composition (Ca/P molar ratio) of synthesized HA and FHA was 1.67. HA was obtained by adding dropwise (3-4 drops) 1.0 M aqueous solution of calcium nitrate tetrahydrate ($Ca(NO_3)_2 \cdot 4H_2O$, Merck, Germany) to 0.6 M aqueous solution of potassium di-hydrogen phosphate (KH_2PO_4, Merck, Germany), under continuous stirring at 2100 rpm for 1 hour at 25°C. The pH was continuously monitored and adjusted to 10 ± 0.1 by adding 25% ammonium hydroxide (NH_4OH, Merck, India) solution to improve gelation and polymerization of HA structure. In case of FHA, a stoichiometric amount of ammonium fluoride (NH_4F, Merck, India) was mixed with KH_2PO_4 solution to maintain P/F ratio at 6 to obtain $Ca_{10}(PO_4)_6OH_{2-x}F_x$ for x=1.

Gels obtained were aged at 25°C for 24 hours. Gelatinous precipitates formed were washed thoroughly by distilled water, centrifuged and dried in an oven at 70°C for 24 hours. The powders were prepared by crushing and grinding the dried gels using mortar and pestle.

2.2. Powder characterization

The morphology and size of nanopowders were observed using TEM (Hitachi, 7500) with resolution of 0.2 nm, operated at an accelerating voltage of 80-100 KV. The powders were ultrasonically dispersed in ethanol to form a dilute suspension and then a drop of suspension was dropped on carbon coated copper grid of 300 mesh for observation.

The BET surface area of powders was evaluated by N_2 adsorption using Quantachrome Instruments NOVA 2200e Surface Area Analyser using Brunauer–Emmett–Teller (BET) method [25]. The linearized form of BET equation is expressed by:

$$\frac{p}{v(p_o - p)} = \frac{1}{v_m z} + \frac{z-1}{v_m z}\frac{p}{p_o} \quad (1)$$

where p/p_0 is the relative vapour pressure of the adsorbate, v is the volume of gas adsorbed, v_m is the volume of gas adsorbed in a monolayer, and z is a constant related to the energy of adsorption. The minimum relative pressure p/p_0 resolution was 2 x 10^{-5}. A linear regression of the left side of BET equation and p/p_0 yields a slope and intercept from which z and v_m are obtained. The BET surface area is then calculated from v_m [26].

XRD (Philips X'Pert 1710) analysis was performed for all powders using Cu K_α radiation, λ = 1.54 Å, 2θ- 20˚ to 80˚, step size 0.017°, time per step 20.03 s, and scan speed 0.005 °/s. Relative amount of different phases present in nanopowders were estimated on the basis of the peak intensity variation by means of external standard method. Both cell parameters, a and c have been calculated using the equation given below [27]:

$$\frac{1}{d^2} = 4/3 \left[\frac{h^2 + hk + k^2}{a^2} \right] + \frac{l^2}{c^2} \quad (2)$$

where d is the distance between adjacent planes in the set of Miller indices (h k l), the reference for HA being JCPDS file no. 09-0432 (a = 9.418 Å, b = 9.418 Å, c = 6.884 Å, space group $P6_3/m$) and for FHA being JCPDS file no. 15-0876 (a = 9.368 Å, b = 9.368 Å, c = 6.884 Å, space group $P6_3/m$. Crystallite size of nanopowders was

calculated using Scherrer's equation [28]:

$$X_s = \frac{0.9\lambda}{\beta \cos \theta} \quad (3)$$

where X_S is the crystallite size in nm, λ is the wave length of X-ray beam, β is the broadening of diffraction line at half of its maximum intensity in radians, and θ is the Bragg's diffraction angle (^{o}). The silicon standard was used to measure the instrument broadening in order to correct the value of β. The three diffraction peaks (0 0 2), (2 1 3) and (2 2 2), which are well separated and have high intensities were chosen to calculate mean crystallite size of hydroxyapatite lattice [29].

FTIR spectra (Perkin Elmer) were recorded in the region 500–4000 cm^{-1} using KBr pellets (1% wt/wt), with spectral resolution of 2 cm^{-1}, taking four scans for each sample.

The thermal behaviour of as-synthesized powders was investigated by TGA/DTG using Mettler Toledo Analytical 2 under following conditions: sample weight 10 mg, heating rate 10 °C/min, peak temperature 1600 °C, and nitrogen gas flow 40 ml/min.

Simulated body fluid (SBF) was prepared in double distilled water using various reagents described by Kukubo [30]. SBF has an inorganic ion composition similar to that of human blood plasma and *in-vitro* experiments can reproduce the reactions that may take place in-vivo [31]. It was kept in polystyrene bottles and placed in a biological incubator at 37.0°C. To study the *in-vitro* behaviour, the HA and FHA nanopowders were immersed individually in SBF solution for 30 days. The change of pH of these SBF solutions was examined under a physiological condition (T= 37.0°C and pH = 7.4) and the pH was measured at an interval of pre-determined time interval using digital pH meter. After 30 days, nanopowders were dried in an oven at 70°C for 4 hrs and were analyzed using TEM and FTIR in the range 400-4000 cm^{-1}.

RESULTS AND DISCUSSION

3.1. Microstructure and BET surface area of nanopowders

The morphology and size of powder particles were determined by TEM observations, in order to evidence the influence of F^- incorporation. In Figures 1a and 1b, TEM micrographs of HA and FHA are shown. The particles of HA consisted of flake- like morphology with length in the range 24 ± 5 nm and width in the range 6 ± 2 nm. FHA powders consisted of rod-like particles having average length as 29 ± 7 nm and diameter as 3.8±0.8 nm, respectively. Due to F^- incorporation in HA lattice, it was found that the morphology changed from flake-like to rod-like.

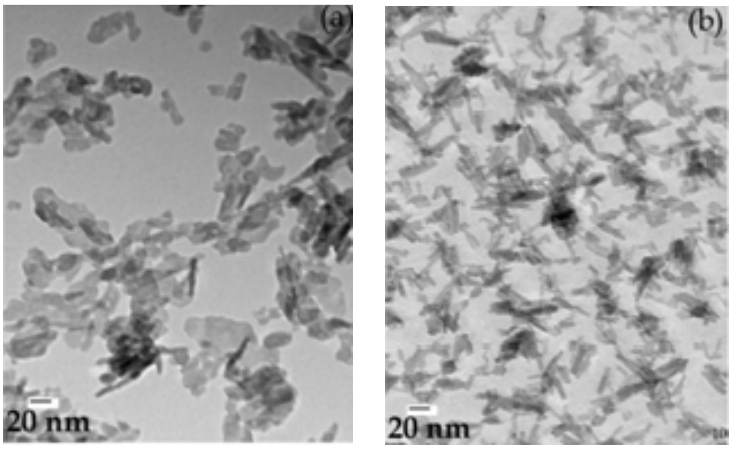

Figure 1: TEM micrographs of (a) HA (b) FHA nanopowders

The BET surface area of nanopowders is presented in Table 1. FHA showed significantly lower BET surface area than HA.

Table 1: BET surface area of nanopowders

Sample	HA	FHA
BET surface area (m^2/g)	205	121

The BET lines for HA, and FHA are shown in Figure 2, the high correlation factor (0.999) giving evidence for the accuracy of BET surface area measurements.

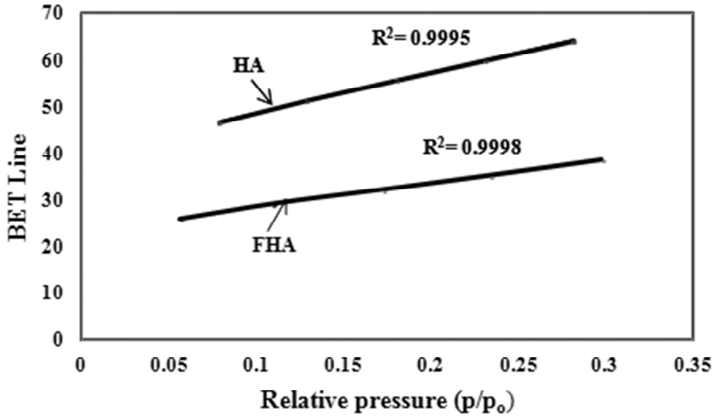

Figure 2: BET lines of HA and FHA nanopowders

3.2. XRD analysis of HA and FHA nanopowders

XRD patterns of HA and FHA powders exhibited almost identical patterns (Figure 3). Both powders consisted of hydroxyapatite and calcium deficient hydroxyapatite (CDHA) phases. The (211) and (112) peaks of FHA merged due to fluorination, which is in agreement with literature [15]. The positions of diffraction peaks for FHA were slightly shifted towards higher angles with respect to HA [32]. FHA showed stronger XRD intensities of apatite compared to HA, indicating that incorporation of F^- ion into the apatite structure enhanced development of apatite phase [33]. The mean crystallite size and lattice parameters of HA and FHA nanopowders are reported in Table 2. On comparing the lattice parameters of FHA nanopowder with HA nanopowder, it was found that substitution of OH- group with F- ion in apatite structure caused changes in 'a' and 'c' lattice parameters because of difference in ionic radius of F^- (1.32 Å) with respect to OH^- (1.68 Å). In the present study, increase in lattice parameter 'c' without significant change in lattice parameter 'a' was observed, indicating the substitution of OH^- with F^- in HA lattice.

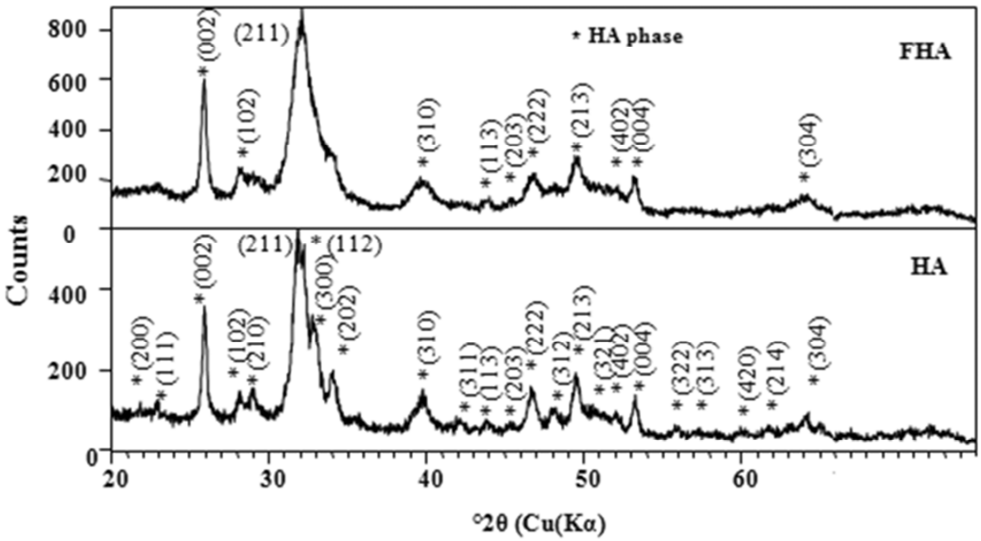

Figure 3: XRD patterns of HA and FHA nanopowders

Table 2: Mean crystallite size and lattice parameters of HA and FHA nanopowders

Nanopowder	Mean crystallite size (nm)	Lattice parameters		
		c (Å)	a (Å)	c/a
HA	34	6.878	9.411	0.728
FHA	22	6.894	9.410	0.730

3.3. FTIR analysis of nanopowders

In Figure 4, FTIR spectra of HA and FHA are reported. Both powders presented the characteristic phosphate vibration of apatites, v_1 PO_4 (962 cm^{-1} in HA and 964 cm^{-1} in FHA), v_3 PO_4 (broad band 1031–1092 cm^{-1} in HA and 1034–1096 cm^{-1} in FHA) and v_4 PO_4 (565 cm^{-1} and 602 cm^{-1} in HA and 565 cm^{-1} and 605 cm^{-1} in FHA). The weak absorption peak at 874 cm^{-1} in nanopowders could be ascribed to P–O–H vibration in HPO_4^{2-} group, typical of CDHA [10]. In HA spectrum, bands existed at 3569 cm^{-1} and 631 cm^{-1} due to the stretching mode of hydrogen bonded OH^- ions. The 3569 cm^{-1} is attributed to a weak hydrogen bond and 631 cm^{-1} is assigned to strong hydrogen bond [34]. These two vibrations in HA spectrum are due to OH^- immersed in an infinite chain of OH^- but this chain is interrupted by F^- in FHA, which is due to the substitution of F^- for OH^- and clearly indicated by absence of these two bands [11, 15]. As the fluoride ion incorporates into the FHA lattice, the band assigned to OH… F… OH appears at 721cm^{-1}.

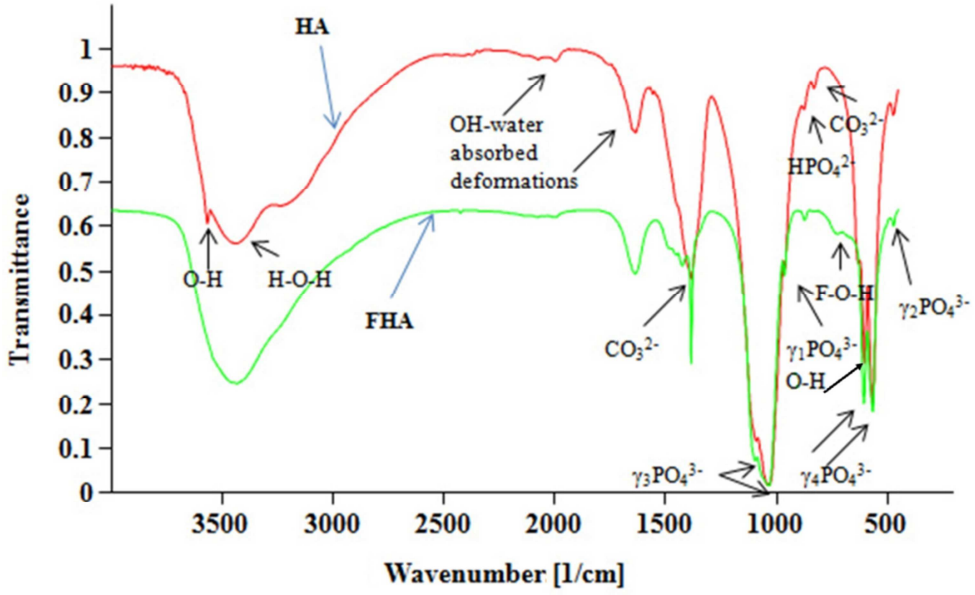

Figure 4: FTIR spectra of HA and FHA nanopowders

3.4. TGA/DSC/DTG analysis of nanopowders

TGA data (Figure 5) combined with DTG and differential scanning calorimetry (DSC) conducted on the as-synthesized nanopowders in the temperature range from 25°C to 1400°C were used to determine the onset temperatures of the loss of OH groups and the decomposition of the HA and FHA nanopowders.

Three weight loss steps are distinguishable in the TGA plot and the corresponding temperature regions are: 25°C to 600°C, 600°C to 1300°C, 1300°C to 1600 °C for HA and 25°C to 380°C, 380°C to 800°C, 800°C to1600°C for FHA. In the first step, the weight loss is due to the evaporation of the adsorbed and lattice water and in the second step the weight loss is due to the release of OH^- groups from HA and FHA crystals.

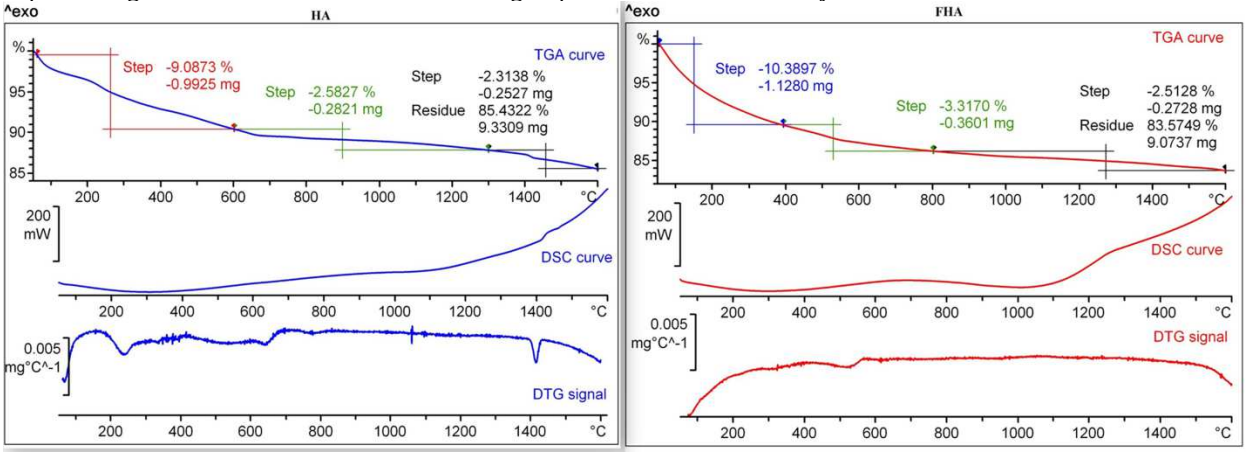

Figure 5: TGA/DTG/DSC curves of HA and FHA nanopowders

The third step weight loss is related to the further decomposition of HA and FHA crystals. On comparing the DTG

signals for HA and FHA, it is noticed that several peaks which appeared for HA disappeared in case of FHA. Most prominent peak around 1400°C seen in case of HA and missing in FHA, further indicates that the F^- substitution in HA enhances its thermal stability. Bogdanova et al. [35] explained high thermal stability of FHA by the difference in the energies of chemical bonds of F^- and OH^- ions with calcium ions in Ca-channels and by structural stabilization.

3.5. In-vitro analysis of nanopowders

In Figure 6, the variation of pH values as a function of immersion time for HA and FHA nanopowders is shown.

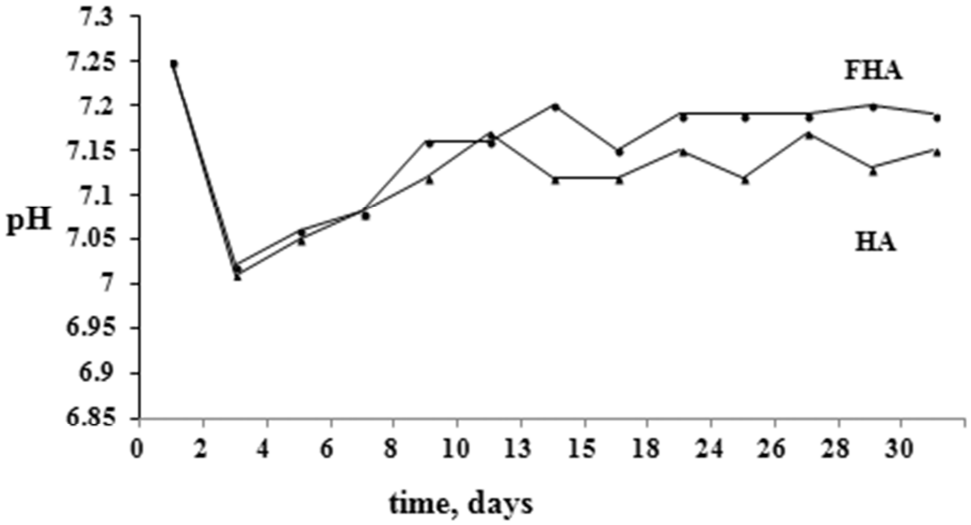

Figure 6: pH changes in SBF with time of immersion for HA and FHA nanopowders

The pH values of SBF solution on immersion of nanopowders rapidly decreased in the initial stage i.e. upto 3 days. As reported in literature [36], the iso-electric point of HA in water is at pH ranging from 5-7, which is lower than pH of SBF i.e. 7.4, the immersion of HA nanopowder in SBF can reveal negative surface charge by exposing its hydroxyl and phosphate ions of its crystal structure. HA nanopowder uses this negative charge to interact with calcium ions in the SBF, consequently forming Ca-rich Amorphous Calcium Phosphate (ACP) layer on its surface. After 3 days, there was an increase in pH value of SBF due to interaction of Ca-rich ACP on the surface of nanopowders with phosphate ions in SBF resulting in formation of Ca-poor ACP layer. The alternate decrease and increase in pH of SBF continued till the period of investigation for HA, whereas for FHA, there was little variation in pH of SBF after 20 days.

TEM micrographs of HA and FHA (Figure 7) after immersion in SBF revealed growth of a layer onto the surface of nanopowders, which might be due to the crystallization of ACP layer as also reported in literature [37].

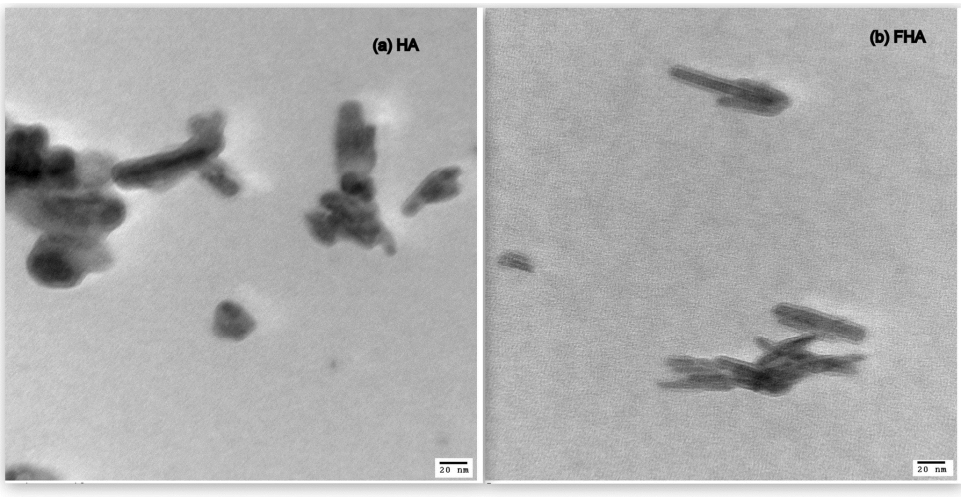

Figure 7: TEM micrographs of HA and FHA dried nanopowders after immersion in SBF solution for 30 days

Figure 8 shows FTIR spectra of HA and Iv-HA (HA immersed in SBF for 30 days) nanopowders and Figure 9 shows FTIR spectra of FHA and Iv-FHA (FHA immersed in SBF for 30 days).

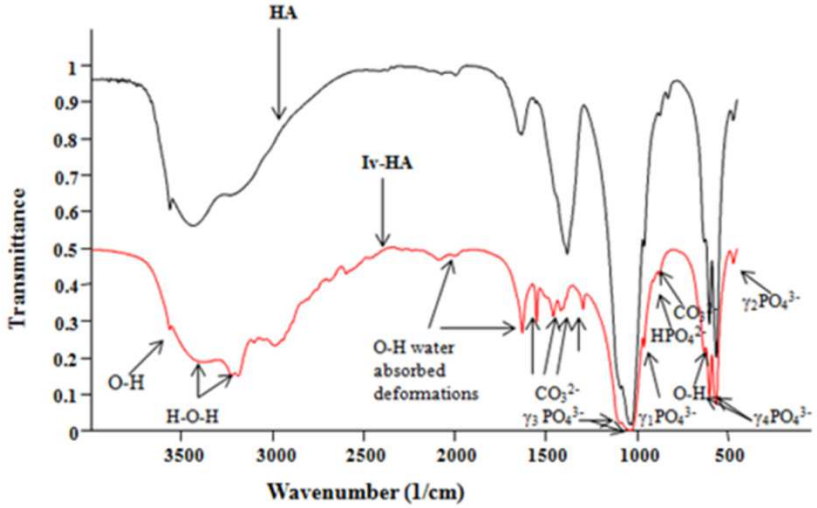

Figure 8: FTIR spectra of HA and Iv-HA

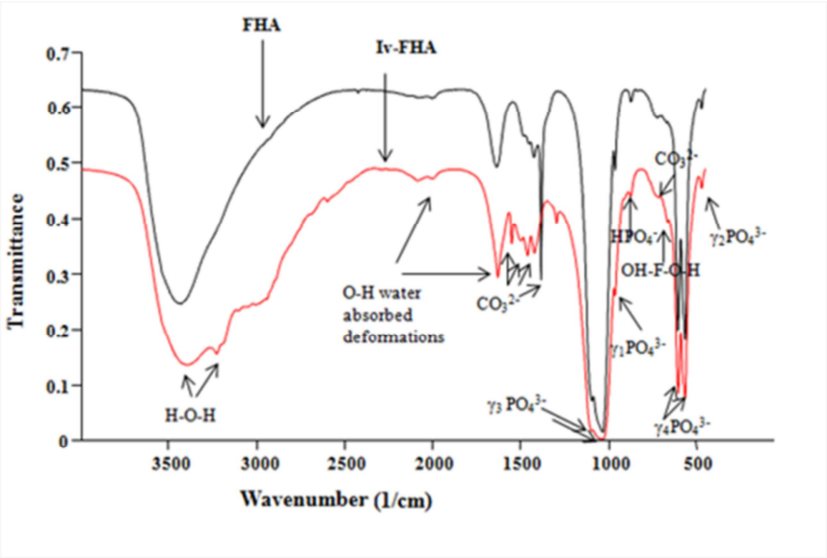

Figure 9: FTIR spectra of FHA and Iv-FHA nanopowders

The FTIR spectra of nanopowders immersed in SBF showed a remarkable decrease in the relative intensities of apatite groups, suggesting that ions from SBF solution deposited a new ACP layer, which is in conformity with the results of pH changes of SBF and TEM results. In Iv-HA and Iv-FHA nanopowders, the additional vibrations (molecular and adsorbed bands) due to the H-O-H bending in H_2O were observed at 3230 cm^{-1} and 1631 cm^{-1}. The γ_3 vibration modes at 1461 cm^{-1} and 1420 cm^{-1} of CO_3^{2-} groups were also observed in FTIR spectra of Iv-HA and Iv-FHA nanopowders, which can be attributed to the dissolution of carbon dioxide from the atmosphere. Since the carbonates are the constituents of the bone structure, the presence of carbonate may improve the bioactivity of nanopowders [38].

CONCLUSION

Nanodimensional HA and FHA powders were successfully synthesized *via* a water based sol-gel route, using a novel phosphorous precursor. HA nanopowder consisted of flake-like agglomerates in comparison to rod-like particles in FHA nanopowder. FHA nanopowder had lower BET surface area than HA nanopowder. The lattice parameters changed due to the substitution of F^- ions into the HA lattice. HA and FHA powders consisted of hydroxyapatite and calcium deficient hydroxyapatite phases. FHA showed higher thermal stability than HA. The HA and FHA nanopowders showed bioactive behaviour *in-vitro*. The fluorine substitution in HA is likely to make it a probable aid in the prevention of dental caries and various bone demineralization disorders, such as osteoporosis, osteomalacia, and periodontal disease. Thus HA and FHA are promising candidates as bone and teeth substitute materials for biomedical applications.

Acknowledgments
This research was funded by Dr. SSBUICET, Panjab University, Chandigarh and PEC University of Technology, Chandigarh under Technical Education Quality Improvement Programme (TEQIP-II). One of the authors (Seema Kapoor) greatly acknowledges the financial support received under UGC Major Research Project, Government of India (F.No.-43-155/2014 (SR)).

REFERENCES

[1] Y Luo; W Li; F Wang; J Zou. *Adv. Mater. Res*., **2011**, 152-153, 1305-1308.
[2] RZ LeGeros. *Adv. Dent. Res*., **1988**, 2, 164-183.
[3] M Niwa; T Sato; W Li; H Aoki. *J. Mater. Sci. Mater. Med.*, **2001**, 12, 277-281.
[4] SM Kenny; M Buggy. *J. Mater. Sci. Mater. Med.*, **2003**, 14, 923-938.
[5] D Norhidayu; I Sopyan; S Ramesh. *ICCBT*, **2008**, 24, 257-270.
[6]B Bracci; P Torricelli; S Panzavolta; E Boanini; R Giardino R; A Bigi. *J. Inorg. Biochem*., **2009**, 103, 1666-1674.
[7] E Landi; S Sprio; M Sandri; G Celotti; A Tampieri. *Acta Biomater.*, **2007**, 4, 656-663.
[8] M Sundfeldt; J Persson; J Swanpalmer; A Wennerberg; J Karrholm; CV Johansson; LV Carlsson. *J. Mater. Sci. Mater. Med*., **2002**, 13, 1045-1050.
[9]KA Bhadang; CA Holding; H Thissen; KM Mc- Lean; JS Forsythe; DR Haynes. *Acta Biomaterialia*, **2010**, 6, 1575-1583.
[10] YChen; X Miao. *Biomaterials*, **2005**, 26, 1205-1210.
[11] LM Rodriguez-Lorenzo; JN Hart; KA Gross. *Biomaterials*, **2003**, 24, 3777-3785.
[12] Y Wang; S Zhang; X Zeng; LL Ma; W Weng; W Yan; M Qian. *Acta Biomater*., **2007**, 3,191-197.
[13] A Bianco; I Cacciotti; M Lombardi; L Montanaro; E Bemporad; Sebastiani. *Ceram. Int.*, **2010**, 36, 313-322.
[14] HW Kim; LH Li; YH Koh; YC Knowles; HE Kim. *J. Am. Ceram. Soc*., **2004**, 87, 1939-1944.
[15] ME Zahrani; MH Fathi; AM Alfantazi. *Metallur. Mater. Trans*. A, **2011**, 42, 3291-3309.
[16] M Darroudi; HE Hosseini; M Housaindokht; Youssefi. *Digest J. Nanomater. Biostruct*., **2010**, 5(1), 29-33.
[17] M Wei; JH Evans; T Bostrom; L Grondahl. *J Mater Sci Mater Med*, **2003**, 14, 311-314.
[18] AJ Nathanael; D Mangalaraj; SI Hong; Y Masuda; YH Rhee; HW Kim. *Mater. Chem. Phys*., **2013**, 137, 967-976.
[19] HG Zhang; Q Zhu; Y Wang. *Chem. Mater*., **2005**, 17, 5824-5830.
[20] H Eslami; M Solati-Hashjin; M Tahriri. *Mater. Sci. Engg. C*., **2009**, 29, 1387-1398.
[21] H Qu; M Wei. *J. Mater. Sci. Mater. Med*., **2005**, 16, 129-133.
[22] F Shafiei; M Behroozibakhsh; F Moztarzadeh; M Haghbin-Nazarpak; M Tahriri. *Micro Nano Letters*., **2012**, 7, 109-114.
[23] N Johari; MH Fathi; MA Golozar. *Ceram. Intern.*, **2011**, 37, 3247-3251.
[24]N Rameshbabu; TS Sampath Kumar; KP Rao. *Bull. Mater. Sci*., **2006**, 29, 611-615.
[25] R Joseph; KE Tanner. *Biomacromol*., **2005**, 6, 1021-1026.
[26] L Clausen; I Fabricius. *J. Colloid Interface Sci*., **2000**, 227:7-15.
[27]TJ Webster; EA Massa-Schlueter; JL Smith; EB Slamovich. *Biomaterials*, **2004**, 25, 2111-2121.
[28] MH Fathi; A Hanifi; V Mortazavi. *J. Mater. Proc. Tech*., **2008**, 202, 536-542.
[29] J Marchi; ACS Dantas; P Greil; JC Bressiani; AHA Bressiani; FA Muller. *Mater. Res. Bull*., **2007**, 42, 1040-1050.
[30] T Kukubo; H Takadama. *Biomaterials*, **2006**, 27, 2907-2915.
[31] C Ohtsuki; T Kokubo; T Yamamuro. *J. Non-cryst. Solids*, **1992**, 143, 84-92.
[32] MH Fathi; E Mohammadi Zahrani. *J. Cryst. Growth*., **2009**, 311, 1392-1403.
[33] K Cheng; G Han; W Weng; H Qu; P Du; J Yang; JMF Ferreira. *Mater. Res. Bull*., **2003**, 38, 89-97.
[34] CY Ooi; M Hamdi; S Ramesh. *Ceram. Int*., **2007**, 33, 1171-1177.
[35] EA Bogdanova; NA Sabirzyanov. *Nanosystems*: *Phy. Chem. Math*., **2014**, 5(4), 590-596.
[36] HM Kim; T Himeno; T Kokubo; T Nakamura. *Biomaterials*, **2005**, 26(21), 4366-4373.
[37] KR Mohamed; HH Beherei; ZM El-Rashidy. *J. Adv. Res*., **2014**, 5, 201-208.
[38] SK Padmanabhan; A Balakrishnan; MC Chu; YJ Lee; TN Kim; SJ Cho. *Particuology*, **2009**, 7, 466-470.